Journal of Chemical Health Risks

www.jchr.org

JCHR (2025) 15(6), 542-553 | ISSN:2251-6727

Spectral Characteristics of ZnO/ Mordent Yellow 12/ Cyclodextrin Nanocrystals

P. Ramasamy[1], A. Mani[1], P. Senthilraja[2], N. Rajendiran[1*]

[1] Department of Chemistry, Annamalai University, Annamalainagar - 608002, Tamil Nadu, India

[2] Department of Bioinformatics, Bharathidasan University, Trichy – 620 024

(Received: 27 September 2025 Revised: 05 October 2025 Accepted: 10 November 2025)

KEYWORDS

Mordant yellow-12, Zinc Oxide nano, Cyclodextrin, Anticancer, Molecular Docking.

ABSTRACT:

The spectral characteristics of ZnO/Mordant Yellow 12/Cyclodextrin nanocrystals were analyzed using UV-Visible, fluorescence, FTIR, DTA, XRD, FE-SEM, and TEM methods. The anticancer activity of MY12 was investigated through molecular docking. MY12 exhibited single emissions in water, α-CD, and β-CD, while dual emissions were observed in nonpolar and aprotic solvents. The PM3 method indicated that the horizontal bond length of MY12 is longer than that of the CD cavities, suggesting partial encapsulation within the CD cavity. The HOMO-LUMO gap for the MY12/β-CD inclusion complex is more negative than that for MY12/α-CD, indicating that the former is more stable. The absorption and fluorescence maxima of ZnO/MY12/β-CD nanoparticles were red or blue-shifted compared to ZnO nano and MY12/CD inclusion complex. Nanoparticle size was measured using TEM-EDS and XRD methods, which revealed that nanocrystals formed in ZnO/MY12/β-CD.

1. Introduction

Nanoparticles of zinc oxide (ZnO) that have diameters less than 100 nanometers. ZnO have been explored for various applications, including drug delivery, biomedicine, bioimaging, and their antibacterial, anticancer, antioxidant, antidiabetic, and anti-inflammatory properties [1-4]. The most common use of ZnO nanoparticles is in sunscreen because they effectively absorb ultraviolet light, but possess a large enough bandgap to be completely transparent to visible light [5]. They are also being investigated to kill harmful microorganisms in packaging [6] and in UV-protective materials such as textiles [7-9]. The aim of the work is, a) to analyse how ZnO nanoparticles interacted with dimethyl yellow-cyclodextrin (MY12:CD) inclusion complex, b) to find which type of nanomaterials is formed, and c) to analyse the anticancer activity of the dye.

2. Material and methods

2.1. Preparation of Drug/CD inclusion complex in solution

Different concentrations of α-CD or β-CD solution (0.1 to 1.0×10^{-2} M) were taken in 10 ml standard measuring flask. MY12 stock solution have a concentration of 2×10^{-2} M and 0.2 ml of the solution was added to the above flasks. The mixed solution was made up to 10 ml with triple-distilled water and shaken very well. The final MY12 concentration in each flask was 4×10^{-4} M and 298 K temperature was used for the experiments.

2.2. Molecular Modeling Studies

Using the molecular modeling software Spartan 08, the molecular geometry of MY12, CD and its inclusion complexes were analysed. The most stable complexation energy was determined theoretically after the structural assembly of two orientation inclusion complexes using the semi-empirical PM3 method in the gas phase and Gaussian 09W software.

2.3. Preparation of ZnO nanoparticles

0.01 M of zinc sulphate was dissolved in 100 ml of deionized water and the solution was heated 50 to 60 °C for 20 to 30 minutes. $ZnSO_4$ and NaOH solution with a molar ratio of 1:2, which was carried out under vigorous stirring for 12 h at room temperature. The obtained white precipitate was washed several times and separated by centrifugation [6–9]. Finally, the precipitate (ZnO) was dried in an oven at 100 °C for 6 h. The prepared ZnO nanoparticles showed a size distribution about 25-50 nm.

Journal of Chemical Health Risks

www.jchr.org

JCHR (2025) 15(6), 542-553 | ISSN:2251-6727

2.4. Preparation of ZnO /MY12/CD nanomaterials

MY12 (2×10^{-3} M) was dissolved in 20 ml of ethanol and gradually added to the CD (1×10^{-2} M in 80 ml) in deionized water. Then 0.01 M zinc sulphate (100 ml) was added to the above MY12/CD inclusion complex solution. Using a hot plate with magnetic stirrer, this mixture was heated to 50 °C for one hour. With vigorous stirring, one to two ml of 1% sodium hydroxide was added and stirred one to two hours. After that, the above solution was frozen and dried (mini-lyophilized) at -80 °C. The powder ZnO/MY12/CD sample was collected and used for further analysis.

2.5. Molecular Docking Method

Auto Dock stands out as a comprehensive software package that employs multiple computational approaches including simulated annealing, local gradient searches, and genetic algorithms [10-15]. Auto Dock 4.2.6 and Auto Dock Vina software were used for the study [13-15]. The docking simulations utilize the Lamarckian genetic algorithm alongside the Solis & Wets local search method. Initial molecular configurations are randomly assigned. Each simulation comprises 10 distinct runs, each limited to 25 x 10^4 energy evaluations, with a population size of 150. The search parameters include a 0.2 Å translational step, with quaternion and torsion steps set at 5 [13-15].

3. Result and Discussion

3.1. UV-Visible and emission spectral studies

Absorption and emission spectral maxima of mordant yellow-12 (sodium 5-[(E)-(4-aminophenyl) diazenyl]-2-hydroxybenzoate **(or)** 5-((4-aminophenyl)azo)-2-hydroxy sodium benzoate, MY12, Fig.1) dye was studied in water, α-CD and β-CD and the related values are given in Table 1, and Fig.2. In water, α-CD and β-CD, the absorption maxima of MY12 were appearing at 380, 251 nm. Upon increasing the CD concentrations, absorption maxima of MY12 are red shifted in α-CD (384, 254 nm) whereas no noteworthy changes noticed in β-CD. However, when increased the concentrations of the α-CD and β-CD, the absorbance of MY12 slightly decreased (Fig. 2).

In water, α-CD and β-CD, MY12 exhibit single emission at 473 nm (Fig. 2). When α-CD or β-CD concentrations raised, no significant spectral shift noticed in the emission however, the intensity regularly increased indicating that MY12 molecule was entrapped into the CD cavities. CD cavity provides a non-polar environment and restricts the free rotation of the MY12 molecule hence, the emission intensity was increased [16-22]. The absorption and emission spectral shifts and shape of MY12 with α-CD or β-CD is same indicate that both CDs are formed similar type of the inclusion complex. From the slope and intercept of the Benesi-Hildebrand plot, the binding constant and stoichiometry ratio of the for the inclusion complexes was determined. The presence of an isosbestic point in the absorption spectrum confirms the formation of a 1:1 inclusion complex [16-22]. The negative free energy change (ΔG) values (Table 1), reveals that the binding process was spontaneous.

3.2. Effect of Solvents

To identify the inclusion complexation process, the absorption and emission spectra of the MY12 was examined in different solvents polarity (Table 1). In MY12, the absorption bond in all the solvents consist of two peaks, which is similar to that observed in 4-aminoazobenzene (4AAB) and azobenzene (AB) [23-27]. The absorption maxima of MY12 (λ_{abs}~ 387, 248 nm, λ_{emi}~ 473 nm) is red shifted than 4AAB and AB molecules (AB, λ_{abs}~ 317 nm, λ_{emi}~ 362 nm, 4AAB, λ_{abs}~ 380 nm, λ_{emi}~ 430 nm). MY12 molecule exhibit single emission in water and CD, while it gives dual emission in nonpolar and aprotic solvents. Due to presence of carboxylate anion may affect the dual fluorescence in water. Absorption maxima of the MY12 molecule is red shifted from non-polar to polar solvents but blue shifted in water, however, in the excited state, the emission maxima red shifted from nonpolar to polar solvents. The data reveal that the position of both bands relatively influenced by nature of the substituent and polarity of the solvents. The absorption and emission spectral shifts are different in the solvents and the CD solution suggest MY12 molecule encapsulated in the CD cavity. The above results reveals that the position and/or the molar extinction coefficient of this band is highly influenced by the nature of the substituents- NH_2 /OH/ COO^-. Because of the greater charge transfer effect of the NH_2/OH groups with the aromatic ring, a large red shift is observed in MY12 than AB.

3.3. Molecular Modeling

Journal of Chemical Health Risks

www.jchr.org

JCHR (2025) 15(6), 542-553 | ISSN:2251-6727

The ground state geometries of MV12, α-CD, β-CD and their inclusion complexes were optimized by the semi-empirical PM3 method. HOMO, LUMO, energy, enthalpy, entropy, free energy, dipole moment, zero-point vibrational energy and Mullikan charge values for the MV12, α-CD, β-CD and the inclusion complexes are given in Table 2. When MV12 entered in to the CD cavity, the polarity and the above parameter values for MV12, α-CD, β-CD significantly changed in the inclusion complexes.

The optimisation procedure was performed for two sets of coordinates, starting either with the aniline ring with azo group (Type I) and salicylic acid ring (Type II) of MV12 molecule encapsulated in the CD cavity. In MY12, the horizontal bond length is 10.77 Å and the vertical bond distance is 4.17 Å (Fig.3). since, MY12 horizontal bond length is longer than the α-CD and β-CD cavity size, this molecule partially encapsulated (i.e., either aniline ring with azo group or salicylic acid ring of the MY12) in the CD cavity. The formation of 1:1 guest/host complexes gain further stabilization energy by hydrogen bonding between hydroxyl groups of the primary and secondary rims of the two different CD molecules. Because of this, the absorption and emission intensities of MV12 in the CD and pure solvents medium shows different results.

The ΔE, ΔG and ΔH values (Table 2) for the MV12/β-CD inclusion complexes is more negative than MV12/α-CD and cavity. The negative Gibbs energy and enthalpy of the inclusion complexes indicate that the formation of the complex is spontaneous and exothermic. The HOMO-LUMO energy orbital pictures of all the inclusion complexes have significantly varied. The blue color indicates for nitrogen atom, while in HOMO-LUMO, the green and red colors denote negative and positive phases of the molecules. The red color in the molecular electrostatic potential's (MEP) figure (Fig.3) shows that the electronegative charge of the atoms is greater than that of other atoms. HOMO-LUMO gap for MV12/β-CD inclusion complex was more negative, which supports that this complex is more stable than Isolated MV12 and MV12/α-CD inclusion complexes.

3.4. Absorption and emission spectral study of ZnO nanoparticles

The absorption and emission spectra of the ZnO, ZnO/MY12, ZnO/β-CD, ZnO/MY12/β-CD nanoparticles are analysed. Absorption and emission band of ZnO nanoparticles appears at 320 nm and 420, 355 nm respectively [28]. When MY12 solution was added to the ZnO nanoparticle solution, the absorption and emission maxima red shifted to 378 nm and 505 nm respectively. With addition of β-CD solution to the ZnO nano, the absorption and emission maxima shifted to 250 and 398 nm respectively. Upon addition of MY12/β-CD solution to the ZnO nanoparticles, the absorption and emission maximum shifted to 360 nm and 495 nm respectively. The above red or blue shifts in the absorption and emission spectra suggest that MY12 and CD covered on the ZnO nanoparticles.

3.5. FE-SEM and EDAX images

ZnO nano, MY12, ZnO/β-CD and ZnO/MY12/β-CD nanomaterials were examined by FE-SEM and EDAX (Fig.4). The morphology images of the above materials demonstrate that all are different shapes. ZnO particles form small size balls present in cluster shape. Morphology of ZnO/β-CD is appear in sheet shape, whereas MY12 present in marble stone shape. However, ZnO/MY12/CD present in croal shape image. The FE-SEM-EDAX data shows the percentage of elements present in the nanomaterials, (a) In ZnO: ~57.34 % zinc, 42.66 % of oxygen, (b) in ZnO/β-CD: 19.67 % of zinc, 54.42 % of oxygen, 25.91 % carbon, (c) MY12 dye contains 62.65 % of carbon, 14.80 % of nitrogen, 21.81 % oxygen, 0.75 % of sodium and (d) ZnO/MY12/β-CD contain 33.3% of zinc, 13.22 % of carbon, 2.61 % of nitrogen, 49.79 % of oxygen and 1.07% of sodium. FE-SEM pictures and the atom composition of the nano ZnO, MY12 are different from ZnO/MY12/β-CD conform the formation of new nanomaterials.

3.6. TEM and EDX images

TEM images of ZnO, ZnO/β-CD and ZnO/MY12/β-CD are displayed in Figs 5. Nano sheet like structures found in the ZnO nanomaterials while nanorod like structure is formed in ZnO/β-CD and nanostone is formed in ZnO/MY12/β-CD. TEM image of ZnO nanosheet were

Journal of Chemical Health Risks

www.jchr.org

JCHR (2025) 15(6), 542-553 | ISSN:2251-6727

seen to uniformly spherical particles between 20 - 44 nm size and in ZnO/β-CD nano, the particles size present between 20 -40 nm. ZnO/MY12/β-CD nano-stone image was displayed to be between 20-33 nm.

The TEM-EDX data predict: (a) ZnO nano contains 69.84 % of zinc nano, 30.16 % of oxygen, (b) ZnO/β-CD nano comprises 8.79 % of zinc, 44.59 % of oxygen and 46.6 % of carbon, (c) ZnO/MY12/β-CD contain 54.78 % of zinc, 9.22% of carbon, 26.36 % of oxygen, 1.98 % of nitrogen and 7.66 % of sodium. The presence of ZnO along with MY12/β-CD is confirmed by the EDX data for the metallic nanoparticles.

The nano particles size is analyzed by X-RD and HR TEM methods. In HR-TEM, the particle size is measured by using IMAGE-J software and the average particle size is calculated by origin software. The particle size is given below: ZnO nano–24.98 nm, ZnO/β-CD–23.98 nm, ZnO/MY12/β-CD nano – 21.30 nm. In XRD method, Scherer equation is used to calculate the particle size: ZnO nano – 19.30 nm, β-CD – 23.84, MY12- 23.71 nm, ZnO/β-CD -20.69 nm, and ZnO/MY12/β-CD Nano –17.19 nm. Compared to XRD method, 3-5 nm particle size is varied in HR-TEM method.

3.7. Powder X-Ray Diffractogram

XRD method provided additional confirmation of the formation of nanomaterials. With the use of the JCPDS: 03-065-3411 data, and the card number 800-075 the mineral name (3C) and the development of the hexagonal closely packed (HCP) structure have been confirmed. The values of the hkl plane are found at (100), (002), (101), (102), (103), (110), (112) and (201) reflection planes of hexagonal structure of ZnO. The XRD peaks are given below:

ZnO :31.80, 34.51, 36.21, 47.52, 56.61, 62.90, 67.91, 69.92

β-CD: 13.39, 19.93, 23.50, 27.65, 31.96, 35.54, 40.58, 48.90

ZnO/β-CD: 10.15, 15.18, 25.41, 28.38, 34.92, 42.29, 49.77, 59.16, 63.32, 70.33

MY12: 27.56, 32.40, 34.57, 46.16, 57.18, 67.05, 76.08,

ZnO/MY12/β-CD: 10.17, 15.02, 25.40, 28.63, 33.21, 34.95, 36.72, 42.38, 49.92, 53.93, 58.95, 63.27, 73.78.

Compared to isolated ZnO, MY12 and β-CD, the XRD patterns of the ZnO/MY12/β-CD nanomaterials showed a different diffraction pattern and different peak intensities suggesting that ZnO/MY12/β-CD nanomaterials were formed.

3.8. Infrared Spectral Studies

FTIR spectra of ZnO nano, MY12, ZnO/MY12, ZnO/β-CD and ZnO/MY12/β-CD are analyzed. The FTIR frequencies of the ZnO nanoparticles were observed at 3325, 1587, 1450, 592, and 513 cm^{-1}. The frequencies appear at 3325 cm^{-1} indicate the presence of ZnO and the peak seen at 592, and 513 cm^{-1} suggest presence of Zn nanoparticles. When β-CD added to zinc oxide nano, the 3325 cm^{-1} frequency shifted to 3280 cm^{-1}, while 1587, 1450 cm^{-1} moved to 1614, 1514 cm^{-1} and 592, 513 cm^{-1} frequencies shifted to 594, 526 cm^{-1}. The above variation in the FTIR frequencies indicate that β-CD covered on ZnO nano particles.

In MY12, the amino and OH group stretching frequency appears at 3340, 3400 cm^{-1}, C=O frequency appears at 1617 cm^{-1}, azo group stretching frequency appears at 1371 cm^{-1}, aromatic ring stretching frequency appear at 1438 cm^{-1}. C-NH_2 frequency appear at 2371 cm^{-1}, and CH out of plane bending frequency appear at 765, 686 cm^{-1}. Out of plane bending frequency appear at 999, 831 cm^{-1} and C-N-C bending frequency appear at 594 cm^{-1}.

When MY12/β-CD added to ZnO nano particles, the above frequencies are shifted to lower or higher wave numbers. In ZnO/MY12/CD, the amino and OH group stretching frequency moves to 3390, 3330 cm^{-1}, C=O frequency moves to 1615 cm^{-1}, azo group stretching frequency appears at 1292 cm^{-1}, aromatic ring stretching frequency appear at 1461 cm^{-1}. C-NH_2 frequency appear at 2360 cm^{-1}, and CH out of plane bending frequency appear at 756 cm^{-1}. Out of plane bending frequency appear at 1035 cm^{-1} and C-N-C bending frequency appear at 594 cm^{-1}. Compared to MY12 and ZnO/β-CD, ZnO/MY12/β-CD nanomaterials showed a marked change in the frequencies suggesting that the ZnO nanoparticles interact with the MY12 and

Journal of Chemical Health Risks

www.jchr.org

JCHR (2025) 15(6), 542-553 | ISSN:2251-6727

encapsulated in the β-CD cavity.

3.9. DTA Thermogram

DTA profiles of pure ZnO nano, MY12, ZnO/β-CD and ZnO/MY12/β-CD are analysed. In ZnO nano, two exothermic peaks noticed at 226.1, and 546.7 °C and three endothermic peaks were observed at 272.6, 731.1 and 919.2 °C. MY12 exhibits one exothermic and one endothermic peak at 240.6 °C and 770.3 °C respectively. β-CD exhibit one exothermic peak at 128.6 °C. In ZnO/β-CD, two exothermic peaks appear at 224.3, and 932.4 °C and four endothermic peaks noticed at 265.2, 354.6, 749.8, and 884.1 °C. In ZnO/MY12/β-CD, three endothermic peak appears at 275.0, 362.3, 813.5 °C, and three exothermic peaks 230.0, 587.9, 946.1 °C. The endothermic peaks in the inclusion complex nanomaterials are caused by the loss of water from the CDs. In contrast to the pure MY12 and ZnO, new peak arises in ZnO/MY12/β-CD conform the formation of the inclusion complex nanomaterials.

3.10. Molecular Docking

The molecular docking analysis was carried out in Dassault Systems BIOVIA Discovery Studio v22.1.100 (licensed version). Three dimensional (3D) structure of our target protein, Epidermal growth factor receptor (EGFR) complex with epiregulin (EREG) was retrieved from Protein Data Bank (PDB) https://www.rcsb.org/(PDBID:5WB7). Protein preparation involved deleting water molecules, ions and adding hydrogen atoms, the docking was performed after grid setup was used to find optimal binding positions.

(EGFR) family consists of four members that belong to the ErbB lineage of proteins (ErbB1-4). Human epidermal growth factor receptor 2 (HER2) is a potent pro-oncogenic heterocomplex. It regulates many crucial cellular programs with different activating ligands determining cell signaling in different ways [29]. Epiregulin (EREG) belongs to the ErbB family of ligands. EREG binds to EGFR and ErbB4 receptor and stimulates homodimers of EGFR and ErbB4 in addition to all possible heterodimeric ErbB complexes, subsequent in the activation of downstream signaling pathways. The EGFR ligands epiregulin (EREG) is stabilize different dimeric conformations of the EGFR extracellular region. EREG is overexpressed in many human cancers and has been concerned in tumor progression and metastasis [30]. So that Epidermal growth factor receptor (EGFR) complex with epiregulin (EREG) was retrieved from Protein Data Bank (PDB ID:5WB7).

Molecular docking of MY12 was given in Fig.6. The figure shows, 3D interactions of Epidermal growth factor receptor (EGFR) complex with epiregulin (EREG) (PDB ID:5WB7) with MY12. The amino acid interaction of target proteins with MY12 are given below: In **2oh4 interacting amino acid residues** - conventional hydrogen bond seen at Cys917 and Lys866, the π alkyl interaction observed at Leu838, Ala864, Val914, Val846 and Leu1033, while π -π stacked interaction seen at Phe916 and the LibDock score is 99.13.

From the autodock method, the following test values are noticed for MY12: ***ADMET solubility level~3*** (***Absorption–Distribution–Metabolism–Excretion–Toxicity*** are the internal processes that describe how a drug moves throughout and is processed by the body), ***ADMET BBB level~1,*** (**Blood Brain Barrier** is a term used to describe the particular properties of the central nervous system (CNS) vasculature), ***ADMET EXT Hepatotoxic applicability# MD~13.09.*** Drug-induced **hepatotoxicity** is an acute or chronic liver injury secondary to drugs or herbal compounds. It is difficult to diagnose. Further, ***ADMET EXT CYP2D6# prediction is true***, ***ADMET EXT Hepatotoxic# prediction is true*** and ***ADMET EXT PPB# prediction is false.*** siRNA plasma protein binding (**PPB**) is a measure of the unbound fraction (f_u) of siRNA in plasma at equilibrium. PPB report is required for small molecule regulatory filing because according to the free drug hypothesis, $f_{u,\ plasma}$ is equivalent to the unbound drug concentration at the site of action at steady state.

4. Conclusion

ZnO/Mordant yellow-12/Cyclodextrin nanoparticles are synthesized and characterized by UV-Visible, fluorescence, FTIR, DTA, XRD, FE-SEM, and TEM methods. MY12 show single emission in water and CD, whereas it gives dual emission in nonpolar and aprotic solvents. The horizontal bond length of MY12

Journal of Chemical Health Risks

www.jchr.org

JCHR (2025) 15(6), 542-553 | ISSN:2251-6727

is longer than the α-CD and β-CD cavities, hence, MY12 partially entrapped in the CD cavity. HOMO-LUMO gap for MY12/β-CD inclusion complex is more negative than MY12/α-CD suggest the previous inclusion complex is more stable than latter. Absorption and fluorescence maxima of ZnO/MY12/β-CD nanoparticles are red or blue shifted than ZnO nano and MY12/CD inclusion complex. Nanoparticle size was measured by TEM-EDS and X-RD methods. TEM image showed nanostones are formed in ZnO/MY12/β-CD. Anticancer activity of MY12 is studied by molecular docking method.

Acknowledgement

This work was supported by the RUSA PHASE -2.0 [No. 128/A1/ RUSA 2.0, Health and Environment] New Delhi, India.

Disclosure statement

No potential conflict of interest was reported by the author(s)

References

1. Kumar, Surabhi Siva, Venkateswarlu Putcha Rao, Vanka Ranga Rao, Gollapalli Nageswara: Synthesis, characterization and optical properties of zinc oxide nanoparticles. International Nano Letters. **2013,** *3,* 30-36.
2. Zhang, Yuanyuan Leu, Yu-Rui Aitken, Robert J., Riediker, Michael: Inventory of Engineered Nanoparticle-Containing Consumer Products Available in the Singapore Retail Market and Likelihood of Release into the Aquatic Environment. International J Environmental Research and Public Health. **2015,** *12,* 8717–8743.
3. Piccinno, Fabiano, Gottschalk, Fadri, Seeger, Stefan, Nowack, Bernd, Industrial production quantities and uses of ten engineered nanomaterials in Europe and the world. J Nanoparticle Research. **2012,** *14,* 1109-1115.
4. Keller, Arturo A, McFerran, Suzanne, Lazareva, Anastasiya, Suh, Sangwon: Global life cycle releases of engineered nanomaterials. J Nanoparticle Research. **2013,** *15,* 1692-1694.
5. Kessler, Rebecca, Engineered Nanoparticles in Consumer Products: Understanding a New Ingredient. Environmental Health Perspectives. **2013,** *119,* A120–A125.
6. Iosub, Cristina Ş, Olăreţ, Elena, Grumezescu, Alexandru Mihai, Holban, Alina M, Andronescu, Ecaterina: Toxicity of nanostructures—a general approach, Nanostructures for Novel Therapy, **2017,** 793–809.
7. Noorian, S A, Hemmatinejad, N, Navarro, JA: Ligand modified cellulose fabrics as support of zinc oxide nanoparticles for UV protection and antimicrobial activities. International J biological macromolecules. **2020,** *154,* 1215-1226.
8. Noorian, Seyyed Abbas, Hemmatinejad, Nahid, Bashari, Azadeh: One-Pot Synthesis of Cu_2O/ZnO Nanoparticles at Present of Folic Acid to Improve UV-Protective Effect of Cotton Fabrics. Photochemistry and Photobiology. **2015,** *91,* 510–517.
9. Hull, Matthew S, Rejeski, David Jr, Hochella, Michael F, McGinnis, Sean P, Vejerano, Eric P, Kuiken, Todd, Vance, Marina E: Nanotechnology in the real world: Redeveloping the nanomaterial consumer products inventory. Beilstein J Nanotechnology. **2015,** *6,* 1769–1780.
10. Morris, G M, Goodsell, D S, Halliday, R S, Huey, R, Hart, W E, Belew, R K, Olson, A J.: Automated docking using a Lamarckian genetic algorithm and an empirical binding free energy function. J. Comput. Chem., **1998,** *19,* 1639–1662.
11. Huey, R, Morris, G M, Olson A J, Goodsell, D S: A semiempirical free energy force field with charge-based desolvation, J. Comput. Chem., **2007,** *28,* 1145–1152.
12. Morris, G M, Lim-Wilby, M: Molecular docking In: Kukol A (ed) Molecular modeling of proteins, Methods in molecular biology, Humana, Totowa, N. J, **2008,** *443,* 365–382.
13. Trott, O, Olson, A J: AutoDock Vina: improving the speed and accuracy of docking with a new scoring function, efficient optimization, and

Journal of Chemical Health Risks

www.jchr.org

JCHR (2025) 15(6), 542-553 | ISSN:2251-6727

multithreading. J. Comput. Chem., **2010,** *31,* 455–461.

14. Anthony D Hill, Peter J Reilly: Scoring Functions for AutoDock, Thomas Lütteke and Martin Frank (eds.), Glycoinformatics, Methods in Molecular Biology, Springer, **1273,** 467-474 (2015)

15. Halgren, Merck, T A: molecular force field. I. Basis, form, scope, parameterization, and performance of MMFF94. J. Comput. Chem., **1998,** *17,* 490-519.

16. Antony Muthu Prabhu, A, Venkatesh, G, Sankaranarayanan, RK, Rajendiran, N: Azonium-ammonium tautomerism and inclusion complexation of 4-amino-2', 3-dimethyl azobenzene, Indian J.Chem., **2010,** *49A***,** 407–417.

17. Antony Muthu Prabhu, A, Venkatesh, G, Rajendiran, N: Azo-Hydrazo tautomerism in 1-phenyazo-2-naphthol dyes in various solvents, pH and β-CD, J. Fluorescence, **2010,** *20,* 961–972.

18. Antony Muthu Prabhu, A, Venkatesh, G, Rajendiran, N: Azonium-Ammonium Tautomerism and Inclusion Complexation of 1-(2,4-diamino phenylazo) naphthalene and 4-Amino azobenzene, J. Fluorescence, **2011,** *21,*1485-1497.

19. Prema Kumari, J, Antony Muthu Prabhu, A, Venkatesh, G, Subramanian, VK, Rajendiran, N: Effect of solvents and pH on β-CD Inclusion complexation of 2,4-dihydroxyazobenzene and 4-hydroxy azobenzene, J. Solution Chemistry, **2011,** *40,* 327–347.

20. Thulasidhasan, J, Rajendiran, N: Host-guest inclusion complexes of propafenone hydrochloride with α- and β-cyclodextrins: Spectral and molecular modeling study, Spectrochim Acta, A, **2013,** *115,* 559–567.

21. Prema Kumari, J, Antony Muthu Prabhu, A, Venkatesh, G, Subramanian, VK, Rajendiran, N: Spectral characteristics of sulfadiazine, sulfisomidine: Effect of solvents, pH and β-CD, Physics and Chemistry of Liquids, **2011,** 49, 108–132.

22. Mani, A, Ramasamy, P, Antony Muthu Prabhu, A, Rajendiran, N: Investigation of Ag and Ag/Co bimetallic nanoparticles with naproxencyclodextrin inclusion complex, J. Mol.Struc. **2023,** *1284,* 135301-10.

23. Sankaranarayanan, RK, Venkatesh, G, Jayashree, E, Pattabiraman, M, Saravanakumar, K, Arivazhznoan, G, Shanmugam, R, Rajendiran, N: Stepwise pesudopolyrotaxane nanostructure formation from supramolecular self-assembly by inclusion complexation of fast violet B with α- and β-cyclodextrins, J.Mol. Struc. **2022,** *1262,* 133080-89.

24. Rajendiran, N, M. Jude Jenita, M, Encapsulation of 4-hydroxy-3-methoxy benzoic acid and 4-hydroxy-3,5-dimethoxy benzoic acid by native and modified cyclodextrins, Spectrochimica Acta, A, **2015,** *136,* 1349–1357.

25. Rajendiran, N, Venkatesh, G, Sankaranarayanan, RK, Dual fluorescence of omeprazole: Effect of solvents and pH, Physics and Chemistry of Liquids, **2014,** *52,* 738-750.

26. Jude Jenita, M, Antony Muthu Prabhu, A, Venkatesh, G, Rajendiran, N, Twisted Intramolecular Charge Transfer effects on fast violet B and fast blue RR: Effect of HP-α-CD and HP-β-CDs, J.Molecular Liquids, **2013,** *178,* 160-167.

27. Antony Muthu Prabhu, A, Suresh Kumar, G.S, Rajendiran, N, Sathiyaseelan, K, Balamathi, M, Interactions between Diphenylamine with 2-Hydroxypropyl β-Cyclodextrin based on Spectral, Biological and Theoretical Investigations. J Macromolecular Science, Part B, **2023,** *63,* 536-569.

28. Sukesh Kashiram Tumram, Rajdip Bandyopadhyaya: Zinc oxide nanostructures: Experiments probing their transformation to nanorods. Materials Science and Engineering: B, **2023,** *296,* 116569-74.

29. Roskoski Jr, R: The ErbB/HER family of protein-tyrosine kinases and cancer. Pharmacological research, **2014,** *79,* 34-74.

30. Sunaga, N, Kaira, K: Epiregulin as a therapeutic target in non-small-cell lung cancer. Lung Cancer: Targets and Therapy, **2015**, *12,* 91-98.

Journal of Chemical Health Risks

www.jchr.org

JCHR (2025) 15(6), 542-553 | ISSN:2251-6727

Table 1. Absorption and fluorescence spectral maxima of MY12 in different Solvents, α-CD and β-CD concentrations

Solvents	**$\lambda_{\alpha\beta\sigma}$**	**log ε**	**$\lambda_{\phi\lambda\upsilon}$**
Cyclohexane	387 248	3.59 3.32	460 430
1,4-Dioxane	387 250	3.59 3.31	460 433
Ethyl acetate	387 255	3.4 3.01	462 427
Acetonitrile	387 250	3.66 3.3	462 429
2-Propanol	385 251	3.58 3.27	469 429
Ethanol	385 251	3.67 3.36	469 429
Water	380 251	3.84 3.57	473
α-CD (0.01 mol/dm^3)	384 254	3.81 3.52	474
β-CD (0.01 mol/dm^3)	380 251	3.78 3.52	475
α-CD K (1:1) x10^5 dm^3/mol	53	-	138
β-CD K (1:1) x10^5 dm^3/mol	143	-	175
α-CD ΔΓ (κχαλμολ^{-1})	-10	-	-12.4
β-CD ΔΓ (κχαλμολ^{-1})	-12.5	-	-13
Excitation wavelength (nm)	-	-	390

Table 2. Energetic features, thermodynamic parameters and HOMO-LUMO energy calculations for MY12 and its inclusion complexes by semiempirical PM3 method.

Properties	**MY12**	**α-CD**	**β-CD**	**MY12/α-CD**	**MY12/β-CD**
E_{HOMO} (eV)	-8.03	-10.37	-10.35	-8.4	-8.22
E_{LUMO} (eV)	-1.26	1.26	1.23	-1.07	-1.09
$E_{HOMO} - E_{LUMO}$ (eV)	6.77	-11.63	-11.58	7.32	7.12
Dipole (D)	9.85	11.34	12.29	13.91	17.18
E (kcal mol^{-1})	-79.7	-1247.62	-1457.63	-1339.95	-1551.98
ΔE (kcal mol^{-1})	-	-	-	-12.63	-14.65
G (kcal mol^{-1})	-148.61	-676.37	-789.52	-827.08	-940.73
ΔG (kcal mol^{-1})	-	-	-	-2.1	-2.6
H (kcal mol^{-1})	-104.65	-570.84	-667.55	-691.48	-790.92

Journal of Chemical Health Risks

www.jchr.org

JCHR (2025) 15(6), 542-553 | ISSN:2251-6727

ΔH (kcal mol^{-1})	-	-	-	-15.99	-18.72
S (kcal/mol-Kelvin)	0.147	0.353	0.409	0.454	0.502
ΔS (kcal/mol-Kelvin)	-	-	-	0.046	0.054
ZPE	136.57	635.09	740.56	773.27	879.93

kcal/mol; **kcal/mol-Kelvin; ZPE = Zero-point vibration energy

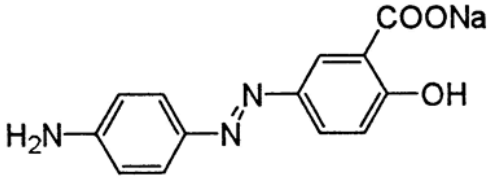

Fig. 1. Chemical structure of Mordant yellow-12 (MY12).

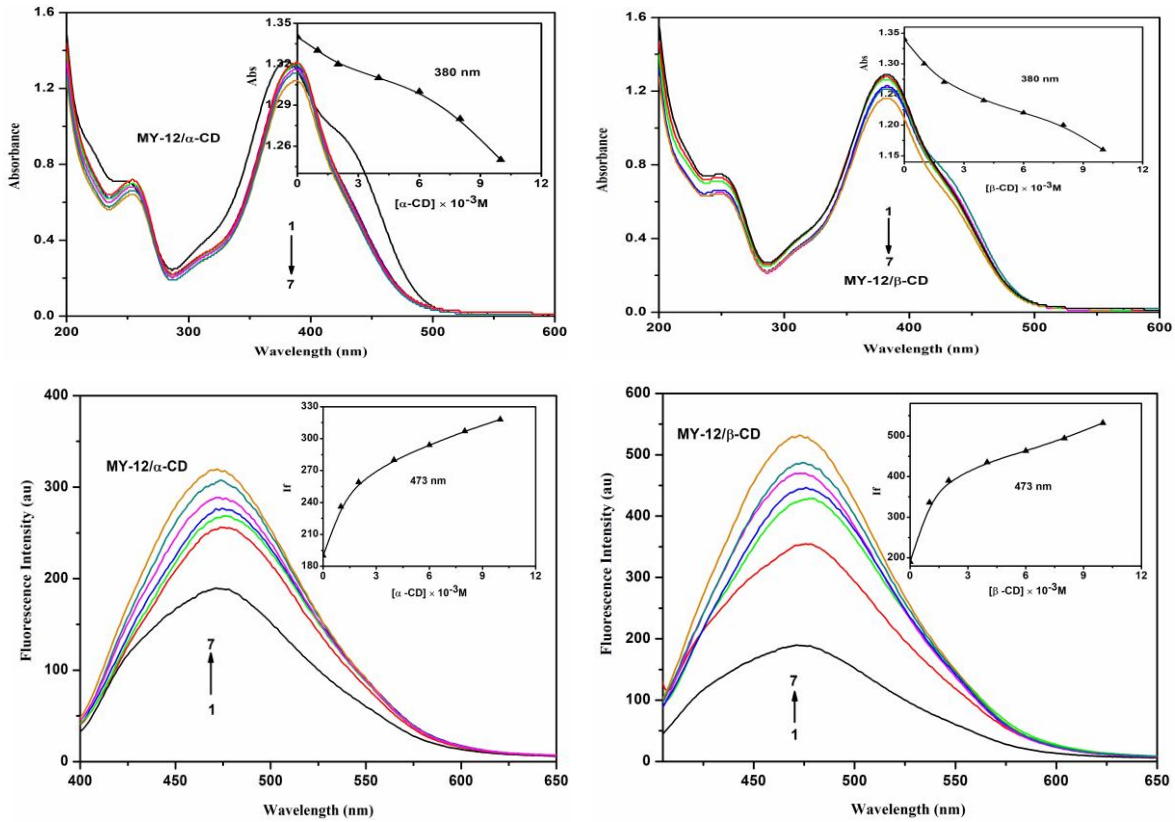

Fig. 2. Absorption and fluorescence spectra of MY12 in different α-CD and β-CD concentrations (mol/dm^3): (1) 0, (2) 0.001, (3) 0.002, (4) 0.004, (5) 0.006, (6) 0.008, (7) 0.01. Insert Figure: fluorescence intensity *vs* [α-CD] and [β-CD].

Journal of Chemical Health Risks

www.jchr.org

JCHR (2025) 15(6), 542-553 | ISSN:2251-6727

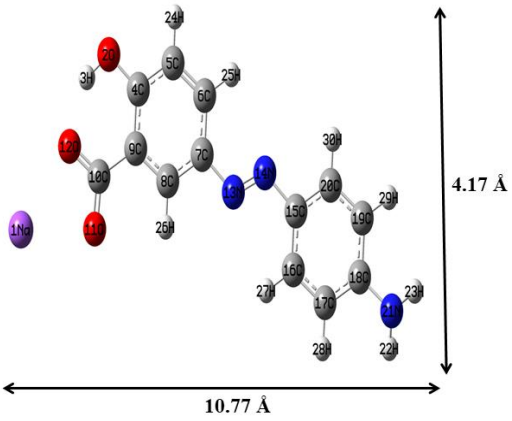

(a) PM3 optimized structure for MY12

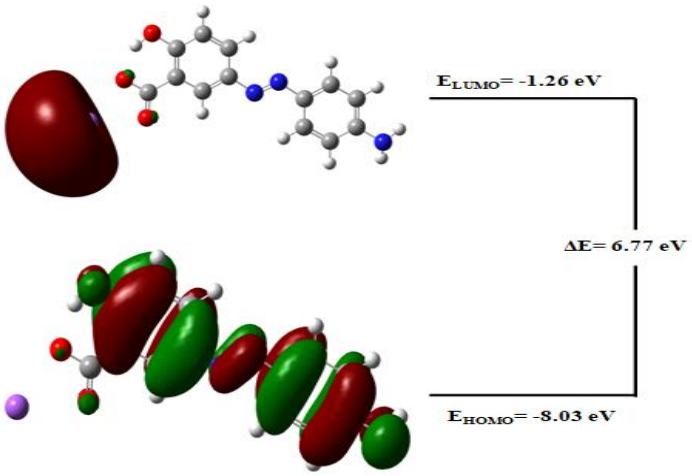

(c) HOMO, LUMO

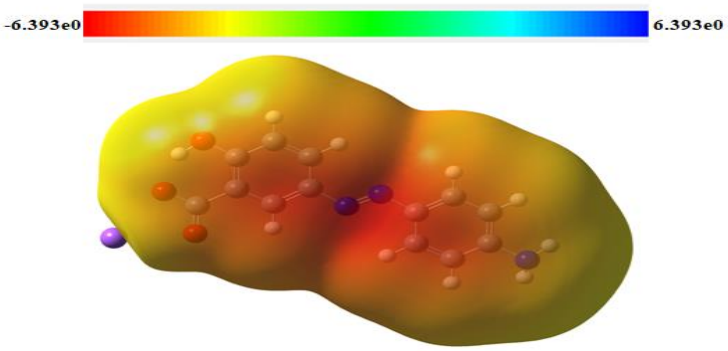

(d) MEP

Fig. 3. PM3 optimized structures of (a) MY12, (b) HOMO, LUMO, (c) MEP of MY12. The blue, red, violet, grey and white colours indicate for nitrogen, oxygen, sodium, carbon and hydrogen atoms respectively. In HOMO-LUMO, the green and red colours denote negative and positive phases of the molecules

Journal of Chemical Health Risks

www.jchr.org

JCHR (2025) 15(6), 542-553 | ISSN:2251-6727

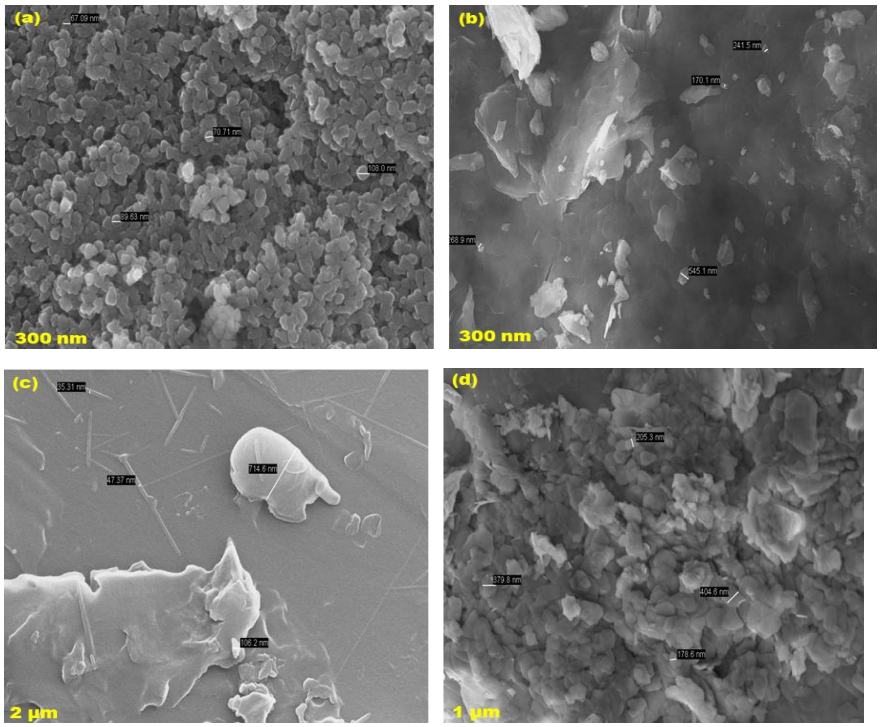

Fig. 4. FE-SEM images for (a) ZnO, (b) ZnO/β-CD, (c) MY12, (d) ZnO/MY12/β-CD.

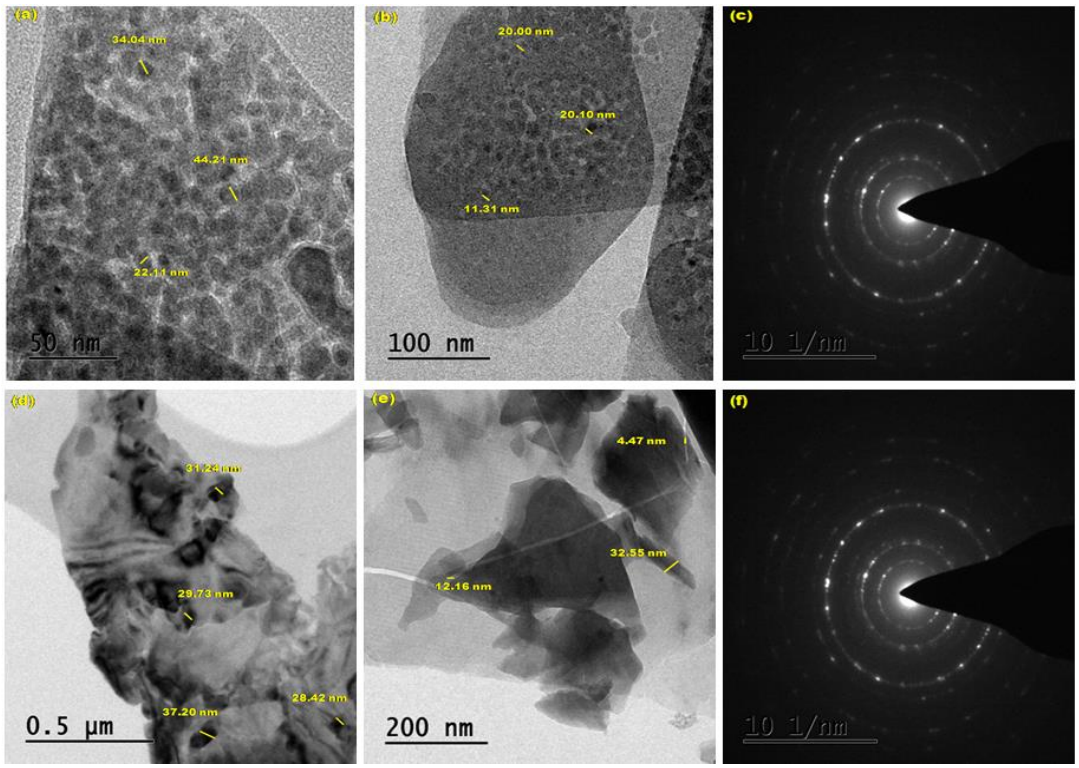

Journal of Chemical Health Risks

www.jchr.org

JCHR (2025) 15(6), 542-553 | ISSN:2251-6727

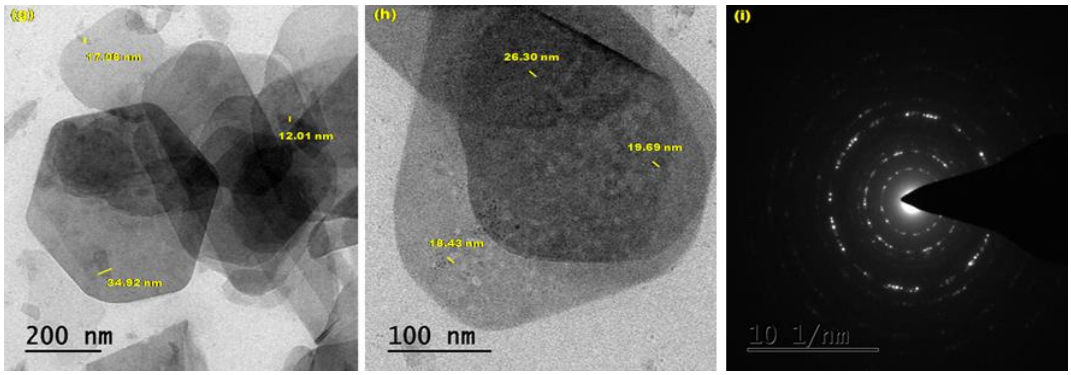

Fig.5. HR-TEM images for (a-c) ZnO, (d-f) ZnO/β-CD, (g-i) ZnO/MY12/β-CD.

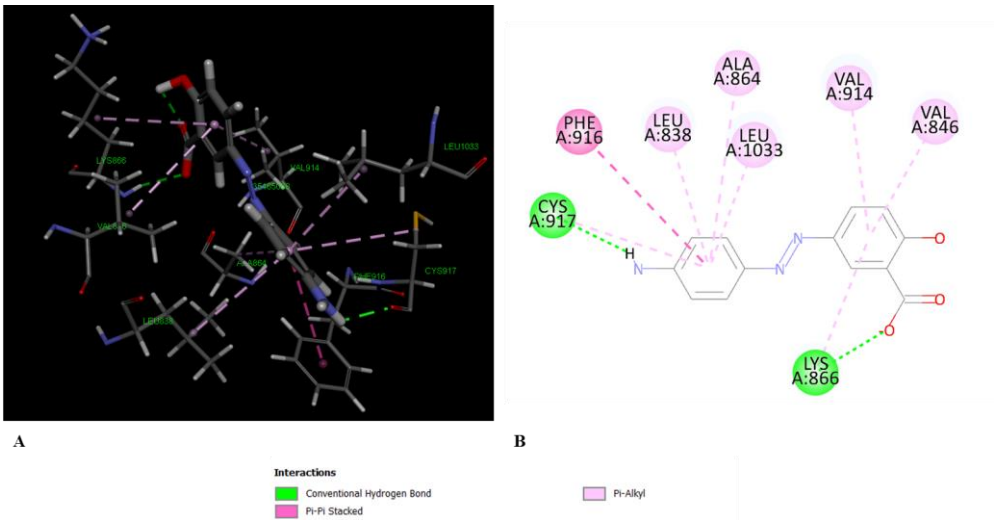

Fig. 6. Molecular Docking – **MY12** interacting with 2oh4 amino acid residues